Comparative Study of Wave Damping on Vertical Wall and Split Chamber Breakwater

Rizaldi C. Yuniardi[1,*], Raka Firmansyah[1], Ika Wulandari[1], Dinar C. Istiyanto[1], Sungsang U. Sujoko[2], Aris Subarkah[2], Shafan A. Aziiz[1], Affandy Hamid[1], Yofan T. D. Harita[1], Suranto[1]

[1]Research Center for Hydrodynamics Technology, National Research and Innovation Agency, Indonesia, 55284
[2]Directorate of Laboratory Management, Research Facilities, and Science and Technology Park, National Research and Innovation Agency, Indonesia, 55284

*Author to whom correspondence should be addressed:
E-mail: riza005@brin.go.id

(Received May 28, 2025; Revised August 04, 2025; Accepted December 17, 2025)

Abstract: Wave damping refers to the reduction of wave energy as it interacts with coastal structures, which plays a crucial role in minimizing potential damage such as shoreline erosion, overtopping, and structural stress on coastal defenses. Coastal protection structures are designed to dissipate wave energy, thereby reducing its impact on shorelines and minimizing the risks of erosion and structural damage. Coastal protection structures may reduce the potential damage caused by wave forces in coastal areas by absorbing wave energy. The Split Chamber is an additional structure comprising multiple chambers installed on the seaward face of a vertical breakwater, designed to enhance wave energy dissipation. This study employs physical modeling to assess the effectiveness of the Split Chamber addition in reducing wave energy, by comparing wave heights in front of a vertical breakwater with and without the Split Chamber. Experimental studies were conducted with sinusoidal regular waves (period T=2.4 s; 3.2 s and height H=4 cm, 8 cm, 12 cm) and irregular waves (period T=2.4 s; 3.2 s and significant wave height Hs=4 cm, 8 cm, 12 cm) in a laboratory scale. Physical modeling results show that the Split Chamber performs greater damping to shorter wave periods for both regular and irregular waves (20.68% for regular wave T=2.4s, 9.73% for regular wave T=3.2 s, 32.06% for irregular wave T=2.4 s, and 24.83% for irregular wave T=3.2 s). Regarding the reflection coefficient (Cr), the split chamber shows a potential reduction of about 10 to 40% for regular waves and about 85% to 100% for irregular waves in comparison to the vertical wall breakwater. The Split Chamber structure can dissipate wave energy by up to 20% at a wave period of 3.2 s.

Keywords: coastal protection; ocean waves; physical modeling; split chamber; wave dissipation

1. Introduction

Differential heating of the Earth's surface drives winds that, when traveling across the ocean, transfer energy to water in the form of surface ocean wind-waves or surface gravity waves. At any point, the wind-wave field is a spectrum of superimposed waves generated by winds from several distributed weather systems, including locally generated wind sea states and long-traveled swells [1)]. Wind-generated ocean waves drive key coastal processes that contribute to erosion and flooding, while coastal regions are also threatened by tsunami waves [2)]. Global wave power, the transport of the energy transferred from the wind into sea-surface motion, has increased globally (and by ocean basins) by 0.4% per year since 1948 [3)]. Climate change significantly drives sea level rise by increasing temperatures that lead to enhanced ice melt and thermal expansion of seawater [4)], resulting in an accelerated global mean sea level rise of 4.4 ± 0.5 mm/year since 2010 due to increased land ice loss and steric changes [5)], and is also associated with a statistically significant increase in maximum wave heights over 84 years, with increments ranging from 0.15 to 0.67 cm/year [6)]. It is important to construct robust coastal protective structures, such as embankments, seawalls, and breakwaters, to protect against wave impacts and coastal inundation [7)]. Enhancing the sustainability performance of port and coastal

Cite: R. Yuniardi et al., "Comparative Study of Wave Damping on Vertical Wall and Split Chamber Breakwater". Evergreen, 12 (04) 2100-2111 (2025). https://doi.org/10.5109/7402640.

infrastructure requires identifying relevant sustainability aspects, defining performance metrics, utilizing quantification tools, and implementing coastal protection measures to mitigate and prevent damage in these areas [8,9]. A seawall safeguards the beach and shoreline against erosion and helps manage water surges resulting from wave activity, whereas a breakwater serves to dissipate and deflect powerful wave energy, which helps to mitigate the effects of wave hazards in coastal environments [10]. Breakwaters of ports establish secure and tranquil water conditions, facilitating safe anchorage and the loading and unloading of ships [11]. The effectiveness of breakwaters is evaluated by analyzing the stability of their structural response, hydraulic performance, wave reflection coefficients, and instances of wave overtopping [12]. Wave reflection from coastal structures and natural coasts creates hazardous sea conditions, accelerates sediment scour, leading to beach sedimentation and erosion, and also structural instability [13–15]. Furthermore, improving the accuracy of predictions for non-dimensional hydraulic parameters deepens our understanding of multi-scale wave interactions and aids in the formulation of sustainable coastal protection strategies to tackle unexpected future challenges [16]. Studies on estimating wave reflection values have been carried out since the 20th century, utilizing both laboratory experiments and theoretical analyses.

Driven by the increased existence of giant ships due to the rapid growth of the maritime logistics transportation industry, there is a growing need for the development of ports with deeper drafts and, concurrently, with a greater height of port breakwater. In deep water settings, rubble mound breakwaters demand extensive horizontal space, which is considered economically inefficient [17]. On the other hand, using caissons in pier walls leads to turbulence in the harbor due to significant wave reflection, which creates unsafe operation conditions for the port [18]. The experiment slotted breakwater consisting of one row of vertical concluded that the wave energy reduction was 20–50% from the incoming wave energy [19].

The idea of hollow caissons was initially presented by Jarlan [20], and subsequently expanded upon by Takahashi [21] and Han & Wang [22]. A range of concepts is continually being refined and adapted to reduce wave forces, minimize reflection while improving stability, address scouring issues at the toe of structures, and also the multi-function designs for Oscillating Water Column (OWC) wave energy converters [23–26]. An examination of wave reflection behaviour through a semi-empirical method [27] experimental and analytical approaches [28], numerical modelling has been conducted [29]. Huang [11] examined the impact of wave refraction mechanisms and wave energy dissipation in Jarlan-type perforated structures, finding that wave reflection on perforated caissons is 20-50% less than that on non-perforated caissons in situations involving irregular waves and overtopping [30]. According to experimental tests conducted by Lee & Shin [31], double-chamber perforated caisson breakwaters (PCB) with reduced porosity in the middle chamber outperform single-chamber caissons in minimizing wave reflection, as opposed to focusing on energy absorption.

However, despite these advancements, a comprehensive understanding of the hydraulic performance of split chamber structures remains limited. Previous studies have not fully compared the wave reflection and damping coefficients of split chamber designs with those of conventional vertical walls under varying wave conditions. This study aims to fill this gap by conducting laboratory experiments using physical models subjected to several combinations of wave period (T) and wave height (H), both regular and irregular waves but did not include tsunamis. The primary objectives are to quantify the wave reflection and damping coefficients of split chamber structures relative to vertical wall structures. The results will provide insights into optimizing coastal protection strategies on a global scale.

2. Method

The present study employs a 1:20 scale laboratory physical model test to investigate the wave damping performance of a Split Chamber structure. The breakwater models, constructed from wood to replicate the geometry of fixed-type coastal structures, were tested under controlled wave conditions. The study compares the wave heights measured immediately in front of the structure for two configurations: a traditional vertical wall breakwater and a modified breakwater with an added Split Chamber. A workflow diagram illustrating the sequential process—from wave simulation with the vertical wall to subsequent testing with the Split Chamber—is presented in Figure 1.

2.1. Experimental setup

The study involved physical model testing in a 2D channel, where a platform was constructed at the channel's base to produce target waves at the location of the structure. [32] highlight that accommodating elevation differences between the channel bed and the platform base requires the inclusion of a transitional slope area when integrating a platform. The platform stands 22 cm high, with a flat length of 16.38 m (3L) and a slope of 1:50, resulting in a total platform length of 29.44 m. Given that the 2D channel length exceeds 34 m, testing can be conducted with a free area of 6.25 m in front of the wave generator (>3-5 m) to create the desired wave conditions at the structure's location [33]. The wave flume utilized in this study is illustrated in Figure 2. During the physical model tests, simulations were carried out at a depth of 28 cm, utilizing two wave period variations (T): 2.4 s and 3.2 s. Each period was tested with three target wave heights (H), repeated three times. The target wave heights included 4 cm, 8 cm, and 12 cm. The types of waves generated were classified

Cite: R. Yuniardi et al., "Comparative Study of Wave Damping on Vertical Wall and Split Chamber Breakwater". Evergreen, 12 (04) 2100-2111 (2025). https://doi.org/10.5109/7402640.

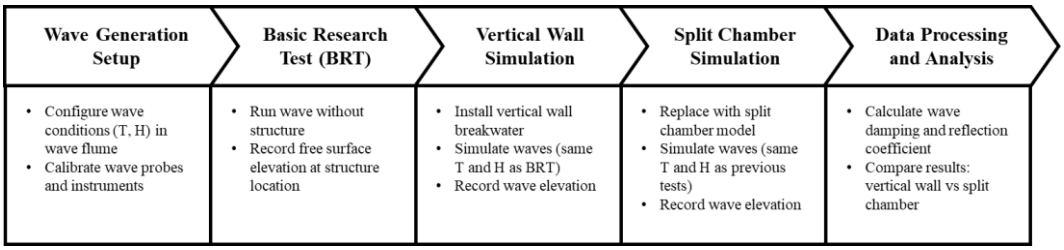

Fig. 1: Flow diagram of the study

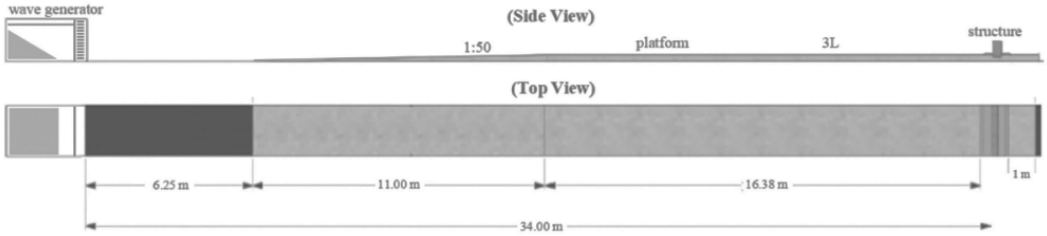

Fig. 2: Illustration of the wave flume

into regular waves and irregular JONSWAP-type waves. For the physical model tests with regular waves, the running time was capped until the reflected waves from the model impacted the structure again (less than three wave cycles), maintaining a distance of 34 m between the wave generator and the structure.

To calculate the specific wavelength, the following iteration formula was used:

$$L = L_0 \tanh(kh) \quad (1)$$

$$L_0 = gT^2/2\pi \quad (2)$$

Where,

L : Wavelength, the horizontal distance between successive crests or troughs of a wave.

L_0 : Deep-water wavelength.

k : wave number.

h : water depth.

g : gravity (9.8 m/s2)

T : wave period

This approach resulted in slight variations in running time for regular waves, depending on the target wave period (T). In the case of irregular waves, the running duration was set to 150 times the number of waves, leading to varied durations depending on the target wave period (T). Table 1 presents the running duration for each test series in the experiment.

The experimental study considered several key variables to evaluate the wave-damping performance of the Split Chamber structure compared to a vertical wall. The primary variables include wave period (T), wave height (H), and structure configuration (vertical wall vs. Split Chamber). Test variations were conducted under different wave conditions, using wave periods of 2.4 s and 3.2 s, with corresponding wave heights set at 4 cm, 8 cm, and 12 cm for both regular and irregular waves. The chamber width-to-structure width ratio (B/L) and chamber height were kept constant, while variations in wave parameters allowed for comprehensive analysis. These variables and test scenarios are summarized in Table 2.

The experimental model adopts Froude scaling to preserve dynamic similarity between the prototype and the model, which is essential for simulating wave motion and fluid-

Table 1: Running duration for each test series

Type of Wave	Period T (s)	Duration (s)	Remark
Regular	2.40	63.58	<3 times of
	3.20	62.77	propagation
Irregular	2.40	360	150 waves
	3.20	480	

Table 2: Wave variables and test scenario

Type of Wave	Wave Period T (s)	Wave Height H (cm)
Regular	2.4	4
		8
		12
	3.2	4
		8
		12
Irregular	2.4	4
		8
		12
	3.2	4
		8
		12

structure interactions in free surface flow environments. A scale ratio of 1:20 was chosen to balance model fidelity and facility constraints. The chamber dimensions were selected based on considerations of functional performance and reference to prior studies on wave dissipation structures. In particular, the B/L ratio and chamber height were set to values that have shown effective wave attenuation in previous experiments [19,30,31]. Additionally, the dimensions were constrained by the geometric limits of the laboratory flume and the need to accommodate a range of wave conditions while ensuring clear comparison with a standard vertical wall structure.

This study focused on the Split Chamber structure with defined parameters. The dimensions of the laboratory model were determined according to scaling principles and the lab's ability to create target waves. The vertical wall structure measures 50 cm in height and 32 cm in width, while the split chamber structure shares the same overall dimensions. At the water surface, the front of the split chamber is divided into two chambers, each measuring 13 cm in height and 16 cm in width. Both structures include toe protection extending 37 cm in length.

2.2. Data acquisition

Eight wave probes were deployed for the test series with T = 2.4 s, and nine probes for the test series with T = 3.2 s, to record water surface oscillations. Wave probes were deployed at intervals equivalent to one wavelength (1L) to capture the complete spatial variability of the wave field since one wavelength encompasses a full cycle of wave motion. Figure 3 illustrates the wave probe arrangement for the T=2.4 s test series and for the T=3.2 s test series. The wave gauge system and data acquisition software used in this study are from HR Wallingford, incorporating HR DAQ software designed for data collection and analysis from physical modeling instruments, including wave gauges. The sampling rate was set to 40 Hz (0.025 s interval), allowing high-resolution time series capture throughout the test duration, which ranged from 60 to 480 seconds depending on the wave period and type. While in Figure 4 presents the cross-section of the structure, featuring both the vertical wall and the split chamber.

Calibration is performed by measuring output variations as the probe is raised or lowered over a known distance in still water. This process utilizes a calibrated stem attached to the wave gauge, featuring a series of precisely spaced holes to ensure accurate adjustment and measurement [34].

3. Result and discussion

3.1. Wave reduction

Basic Research Test (BRT) was performed to identify the capability of the wave generator to produce incoming waves with the target heights as defined in the testing scenarios (Table 2). The results of the BRT are presented in Table 3 and for the calibration results of the wave probes, along with the corresponding R^2 values for each probe, are presented in Figure 5 and Table 4. These results confirm the successful calibration of the sensors, demonstrating their accuracy and reliability for experimental testing [34].

The Basic Research Test revealed the necessary input waves for the wave generator to generate the target waves

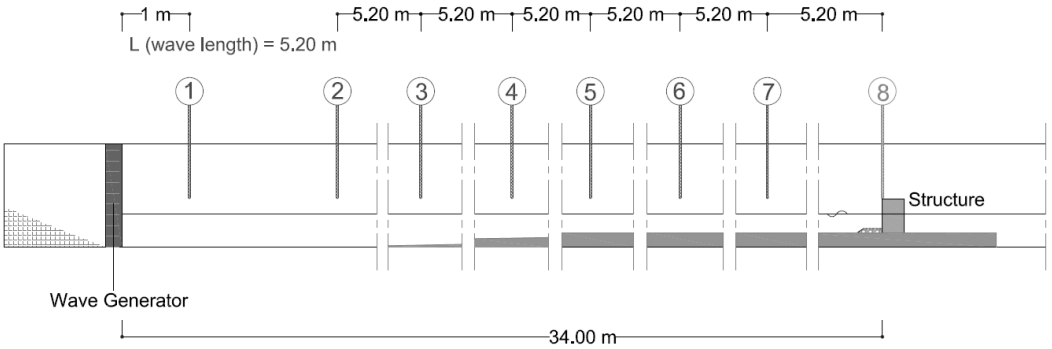

(a)

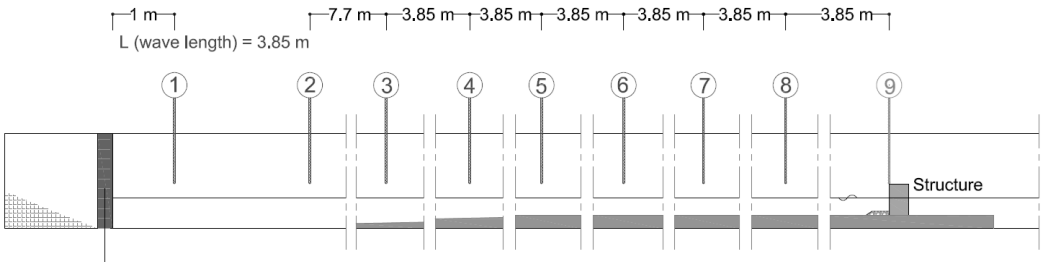

(b)

Fig. 3: Wave probe arrangement for the test series of (a) T=2.4 s and (b) T=3.2 s

Cite: R. Yuniardi et al., "Comparative Study of Wave Damping on Vertical Wall and Split Chamber Breakwater". Evergreen, 12 (04) 2100-2111 (2025). https://doi.org/10.5109/7402640.

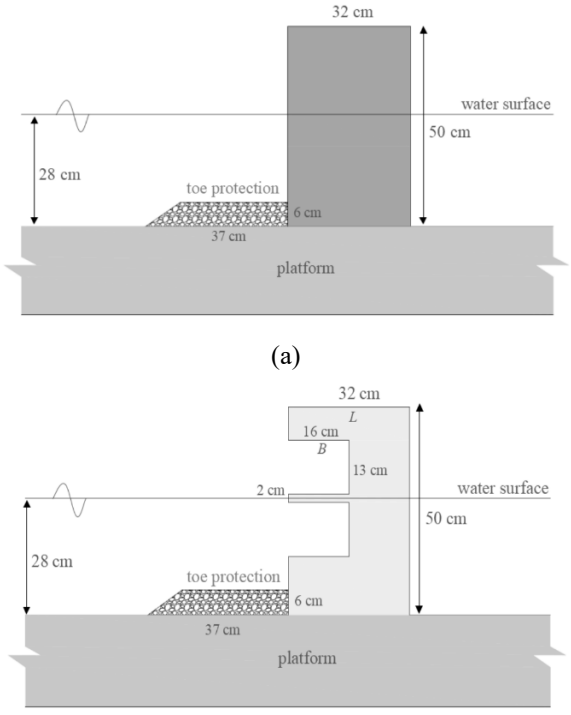

Fig. 4: Cross section of the structure for (a) vertical wall and (b) split chamber

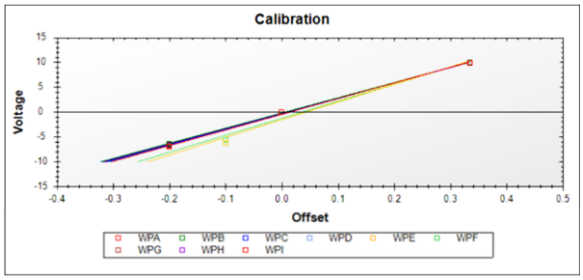

Fig. 5: Calibration graph's result of each probe

Table 4: R^2 values form calibration's result of each probe

No	Wave Probe	Sensor Name	R^2
1	WP 1	WPA	0.9978
2	WP 2	WPB	0.9995
3	WP 3	WPC	0.9989
4	WP 4	WPD	0.9981
5	WP 5	WPE	0.9987
6	WP 6	WPF	0.9989
7	WP 7	WPG	0.9994
8	WP 8	WPH	0.9991
9	WP 9	WPI	0.9995

Table 3: Results of basic research test

Type of Wave	T (s)	H_{target} (cm)	H_{input} (cm)	WP at Structure Location		Diff (%)	Remark
				H_{output} (cm)	T_{output} (s)		
Regular	2.40	4.00	3.90	3.99	2.40	-0.25	WP9 ; $\bar{H}$ and $\bar{T}$
		8.00	7.20	7.98	2.39	-0.25	
		12.00	10.30	11.94	2.38	-0.50	
	3.20	4.00	3.60	4.05	3.19	1.25	WP8 ; $\bar{H}$ and $\bar{T}$
		8.00	6.55	7.90	3.19	-1.25	
		12.00	9.30	11.98	3.19	-0.17	
Irregular	2.40	4.00	4.15	4.00	2.50	0.00	WP9 ; H_s and T_p
		8.00	8.52	7.90	2.44	-1.25	
		12.00	13.03	11.30	2.94	-5.83	
	3.20	4.00	3.77	4.00	3.23	0.00	WP8 ; H_s and T_p
		8.00	7.72	8.00	3.23	0.00	
		12.00	11.75	11.20	3.23	-6.67	

at the structure's location. With a maximum differentiation of 1.25%, further testing was conducted using these inputs to analyze wave behavior on both the vertical wall and Split Chamber structures. Results showing a differentiation greater than 1.25%, particularly for the highest target wave of the irregular wave type, were still utilized for comparison of the reflection coefficient. The water profile observed in front of the vertical wall and split chamber during the ongoing experiment is presented in Figure 6.

Data collection took place in a 2D channel, featuring various test series based on different parameters and wave types. To validate the findings, physical model tests were conducted with multiple repetitions (three for each wave height tested). The outcomes of these repetitions produced the standard deviations ($\overline{SD}$)), as presented in Table 5.

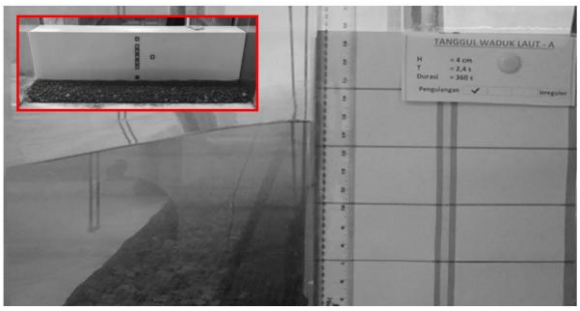

(a)

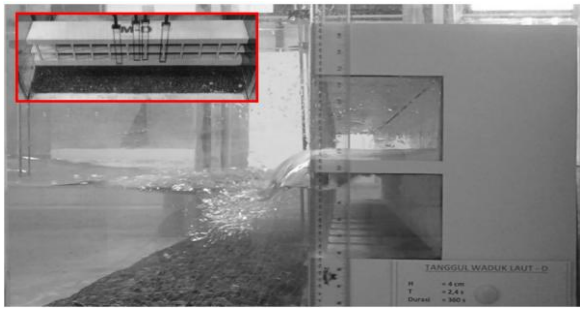

(b)

Fig. 6: Side view of the water profile in front of the structure in the ongoing experiment for (a) vertical wall and (b) split chamber

Table 5: Results of the experiment

Type of Wave	T (s)	H (cm)	Standard Deviation
Regular	2.4	4	0.05
		8	0.13
		12	0.11
	3.2	4	0.02
		8	0.07
		12	0.16
Irregular	2.4	4	0.21
		8	0.12
		12	0.29
	3.2	4	0.03
		8	0.24
		12	0.22

In the simulations involving regular waves, the parameters utilized and analyzed are the average wave height ($\bar{H}$) and average wave period ($\bar{T}$).

Before data processing is carried out to obtain wave parameters such as wave height and wave period, the time series samples reveal fundamental differences in the vertical structure between the wall and the split chamber, In regular waves, after the wave reaches the target BRT wave, the vertical wall structure generates a standing wave effect, resulting in the wave height doubling, whereas the both in regular and irregular waves as shown in Figure 7. split chamber structure mitigates this phenomenon through

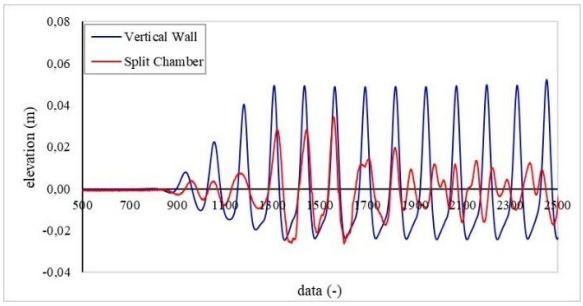

(a)

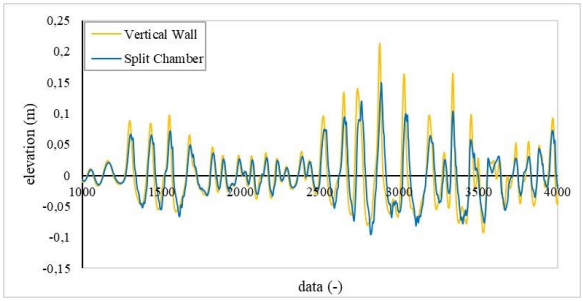

(b)

Fig. 7: Time series samples at the structure for (a) Regular waves T=3.2 s; H=4 cm, and (b) Irregular waves T=3.2 s; H=8 cm

its chamber design. In irregular waves, the wave formation is highly random, making it impossible to observe the persistent and stagnant standing wave phenomenon.

In Figure 8**Error! Not a valid bookmark self-reference.**, a graph is presented comparing the experimental results of the BRT, vertical wall, and split chamber across all wave probes for regular wave conditions in the T=2.4s series, with variations in wave height. In the tests with regular waves having a period (T) of 2.4 s and an average standard deviation ($\overline{SD}$) of 0.09 across three repetitions, it was observed that the wave height at the Split Chamber structure's location differed from that at the vertical wall structure ($\bar{H}$ in front of the Split Chamber < $\bar{H}$ in front of the vertical wall structure). For a target wave height of 4.00 cm from the BRT at the structure location, the height rose to 8.08 cm (with an average $\bar{T}$ of 2.39 s) when using a vertical wall structure

(Cr ≈ 1). In contrast, when the Split Chamber structure was used, the wave height was 6.52 cm (with an average $\bar{T}$ of 2.4 s), indicating a damping effect of this structure relative to the vertical wall structure of approximately 19.38%.

In Figure 9, a comparison of the experimental results for the BRT, vertical wall, and split chamber is shown across all wave probes under regular wave conditions in the T=2.4 s and T=3.2 s series, with varying wave heights. The damping effect of the Split Chamber structure compared to the vertical wall for a target wave height of 8.00 cm (T=2.4 s) from the BRT is 20.75%, and for a target wave height of 12.00 cm, it is 21.92%. In a separate test with a wave period of T=3.2 s and an average standard deviation ($\overline{SD}$) of 0.08 across three repetitions, the damping effectiveness

of the Split Chamber structure relative to the vertical wall

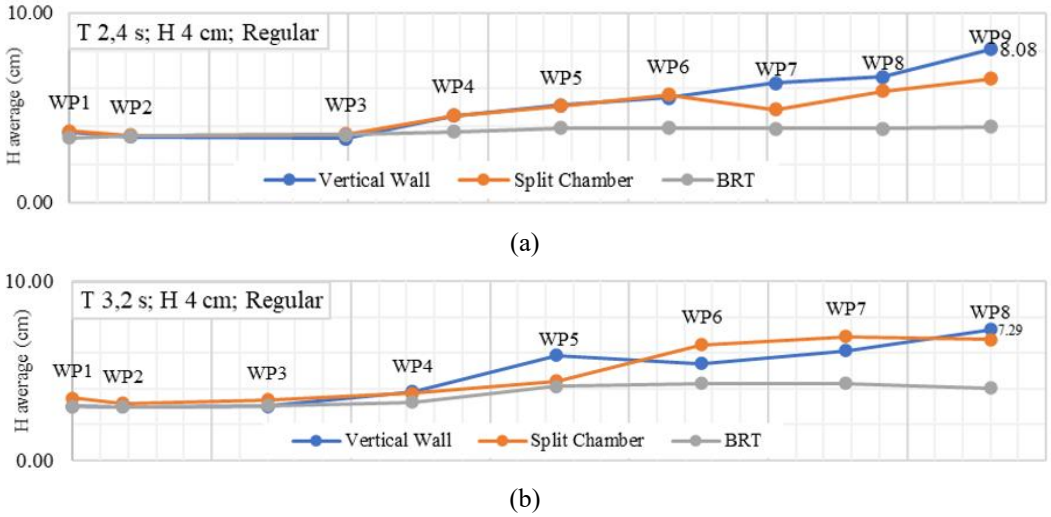

Fig. 8: Graph of the sample results of the experiment comparing BRT, vertical wall, and split chamber for each wave probe for regular wave at H=4 cm series with (a) T=2.4 s and (b) T=3.2 s

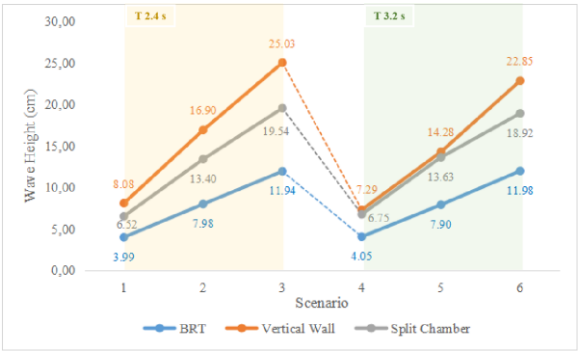

Fig. 9: Graph of the results of the experiment comparing BRT, vertical wall, and split chamber for regular wave

structure was 7.41%, 4.58%, and 17.21% for target wave heights of 4 cm, 8 cm, and 12 cm, respectively. These damping values are lower than those recorded for the 2.4 s period. This suggests that for regular waves, a shorter wave period (T) enhances the damping capability of the Split Chamber structure.

For the simulations involving irregular waves, the parameters analyzed include the significant wave height (Hs) and the peak wave period (Tp).

The experimental results for the BRT, vertical wall, and split chamber are compared across all wave probes under irregular wave conditions in the T=2.4 s and T=3.2 s series, as shown in Figure 10. In the irregular wave tests with a wave period (T) of 2.4 s and an average standard deviation ($\overline{SD}$)of 0.21 across three repetitions, it was observed that the wave height at the Split Chamber structure location differed from that at the vertical wall structure (Hs in front of the Split Chamber < Hs in front of the vertical wall structure). In the analysis of irregular data, to establish an energy equivalence with regular waves, the significant wave height is divided by $\sqrt{2}$. For a target wave height of 4.00 cm from the BRT at the structure, the height rose to 8.27 cm (with an average Tp of 2.38 s) when a vertical wall structure was employed. In contrast, when the Split Chamber structure was used, the wave height decreased to 5.38 cm (with an average Tp of 2.4 s), indicating a damping effect of this structure compared to the vertical wall structure of about 34.91%.

The experimental results for the BRT, vertical wall, and split chamber are shown for all wave probes under irregular wave conditions in the T=2.4 s and T=3.2 s series in Figure 11. The damping effect of the Split Chamber structure compared to the vertical wall for the BRT target wave height of 8.00 cm is 34.24%, and for the target wave height of 12.00 cm, it is 27.03%. In a separate test with a wave period of T = 3.2 s and an average standard deviation ($\overline{SD}$) of 0.16 across three repetitions, the damping effectiveness of the Split Chamber structure compared to the vertical wall structure was recorded at 23.92%, 22.60%, and 27.96% for target wave heights of 4 cm, 8 cm, and 12 cm, respectively. These damping values are lower than those observed for the 2.4 s period. This suggests that, similar to the regular wave tests, shorter wave periods (T) also improve the damping capacity of the Split Chamber structure in the context of irregular waves.

In general, the wave height in front of the split chamber structure is lower than the wave height in front of the vertical wall structure, given the same BRT wave height (at the location before the structures are present), according to the analysis results using regular and irregular waves on the two tested structures, which are the split chamber and the vertical wall, as shown in Figure 12. The split chamber's wave height in relation to the vertical wall, or wave damping, ranges from 4.58% to 34.91%. By creating an approximate equation using power regression to forecast the wave heights that would occur for both

structures based on the test data that is currently available, this discovery can be further investigated. The scale coefficient or proportionality factor of the equation derived

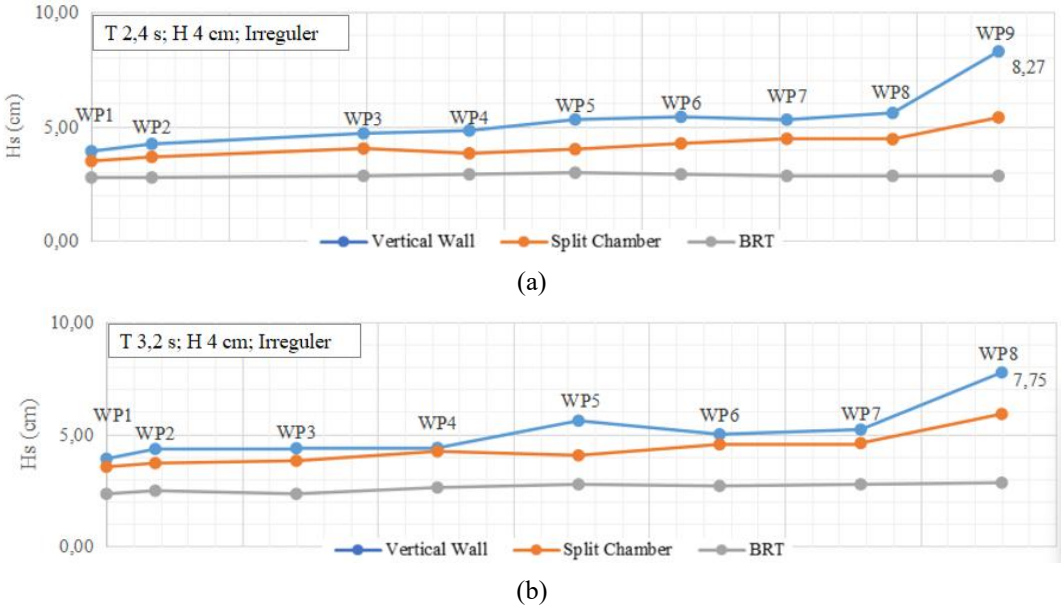

Fig. 10: Graph of the sample results of the experiment comparing BRT, vertical wall, and split chamber for each wave probe for irregular wave at H=4 cm series with (a) T=2.4 s and (b) T=3.2 s

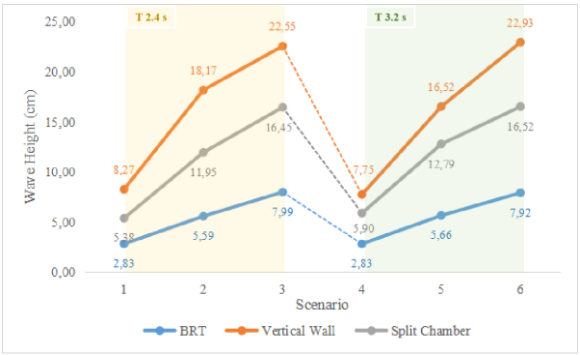

Fig. 11: Graph of the results of the experiment comparing BRT, vertical wall, and split chamber for irregular wave

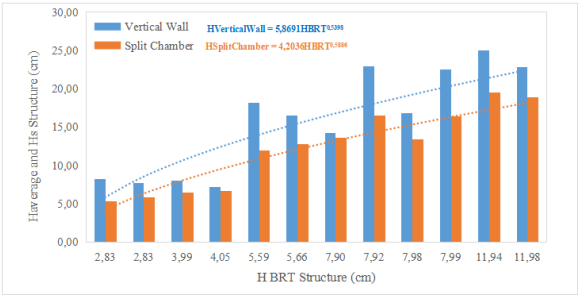

Fig. 12: Graph of the results of the experiment comparing vertical wall and split chamber for all scenarios

for the vertical wall structure is 1.38, which is greater than that of the split chamber structure.

3.2. Wave reflection

Previous studies have extensively examined the influence of dimensionless width-to-wavelength ratios (B/L) on wave reduction and energy dissipation. Pereira et al. [35] demonstrated that a B/L ratio of 0.23 significantly enhances wave attenuation, achieving a 90% reduction in design wave height. Furthermore, their findings indicated that the energy reflected from the structure could be limited to approximately 25%, with the structure dissipating up to 70% of the incident wave energy.

Similarly, Fang He [36] observed that a B/L ratio of 0.207 achieved a maximum reflection coefficient (Cr) of 0.29, highlighting its effectiveness in reducing wave reflection, with experimental results showing that the incident wave could be effectively attenuated by the structure. Kirca [37] further contributed to this understanding by showing that structures with B/L ratios in the range of 0.2–0.3 reduced wave impact by approximately 35%–40% under regular wave conditions. Kirca also noted that shorter waves and wider chambers tend to diminish the wave loads exerted on the structure. In contrast, very narrow chambers (B/L=0.06) increased wave loads, even exceeding those on a plain vertical structure.

These findings collectively underline the critical role of B/L ratios in optimizing wave energy management and minimizing structural loads, emphasizing the need for careful consideration of chamber breadth and wave characteristics in design processes.

In his study indicates that in the tests with irregular waves, the Split Chamber structure demonstrates a greater damping capacity than in the regular wave tests. This is attributed to the fact that the irregular wave simulations were carried out over 150 wave cycles, allowing the waves to experience more than three cycles of propagation, which resulted in significant reflections from the structure,

particularly from the vertical wall structure lacking dampers. The reflection coefficient (Cr) is calculated using wave heights measured at the structure's location during the Basic Research Test—denoted as H for regular waves

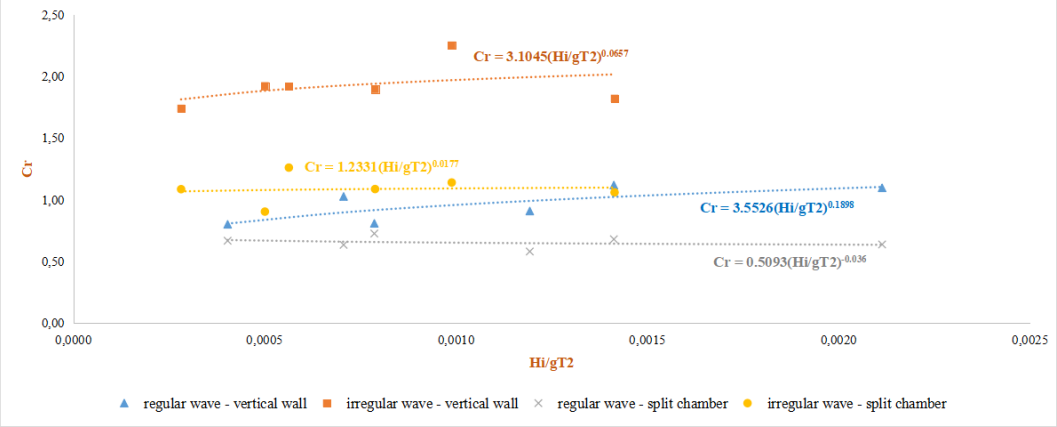

Fig. 13: Correlation between reflection coefficient (Cr) and the ratio of $\bar{H}$ and Hs from the BRT in relation to the wave period and gravity

and Hs for irregular waves—and during the test with the structure in place. The specific calculation methods are detailed in formula below.

$$Cr_{(reg)} = \frac{\bar{H}_{in\ front\ of\ the\ structure} - \bar{H}_{BRT\ at\ the\ loc.of\ the\ structure}}{\bar{H}_{in\ front\ of\ the\ structure}} \quad (3)$$

$$Cr_{(irreg)} = \frac{Hs_{in\ front\ of\ the\ structure} - Hs_{BRT\ at\ the\ loc.of\ the\ strucure}}{Hs_{in\ front\ of\ the\ structure}} \quad (4)$$

The relation between the reflection coefficient and the ratio of $\bar{H}$ and Hs from the Basic Research Test in relation to the wave period and gravity, representing a non-dimensional analysis, is illustrated in Figure 13.

The nondimensional relationship between the reflection coefficient and wave height relative to wavelength is determined using power regression. By analyzing two types of waves across two tested structures, it is observed that the reflection generated by irregular waves is greater than that of regular waves in both vertical wall and split chamber structures ($C_r = 3.1045(H_i/GT^2)^{0.0657}$ over $C_r = 1.2331(H_i/GT^2)^{0.0177}$ for vertical wall structure). For the same target wave height at the location of the structures in BRT, irregular waves exhibit a higher average third-wave reflection than the average reflection of regular waves. Additionally, the reflection trend for vertical wall demonstrates higher values compared to split chamber structures. Waves interacting with the split chamber structure, which functions as a wave dissipator, result in lower reflected wave heights. This reduction is attributed to the limitation imposed by the chamber height of the tested structure. Irregular waves are represented as significant waves (Hs), which means these waves represent the average of the highest one-third of waves in their time series. This implies that the presence of individual waves larger than others within the spectrum generated during the testing will inevitably result in higher wave amplitudes when interacting with the structure, particularly a vertical wall structure. These nonlinear effects can amplify wave heights, particularly when the waves encounter a structure. With this larger Hs, the resulting Cr value (reflection coefficient) is also greater, even though the energy has been equivalenced to that of regular waves.

The split chamber structure effectively reduces wave reflection compared to vertical wall designs due to its unique mechanism of energy dissipation through flow separation and internal circulation. The separation between upper and lower chambers facilitates energy absorption within the structure, significantly lowering wave reflection coefficients [38,39]. Additionally, the internal circulation of water dissipates incident wave energy, reducing the energy available for reflection [29]. This design enhances the structure's ability to attenuate wave forces, minimize wave loads, and improve stability under irregular and resonant wave conditions.

Vertical wall structures, while effective, often lead to higher wave reflection due to their rigid design, which limits energy dissipation. In contrast, split chamber structures are more effective at reducing reflected wave height by dissipating wave energy through flow dynamics within the chambers. This comparison underscores the critical importance of structural design in managing wave energy and optimizing performance under challenging wave conditions.

4. Conclusion

This research utilized physical model testing to evaluate the wave-damping effectiveness of the Split Chamber structure in comparison to the vertical structure. The experiments included various test series with different wave heights, wave periods, and wave types. The result

Cite: R. Yuniardi et al., "Comparative Study of Wave Damping on Vertical Wall and Split Chamber Breakwater". Evergreen, 12 (04) 2100-2111 (2025). https://doi.org/10.5109/7402640.

indicates that the split chamber structure consistently reduces wave reflection and enhances energy dissipation, with its performance varying based on wave characteristics. For regular waves, the structure exhibited a damping ranging from 19% to 21% for shorter wave periods (T=2.4s) while for longer wave periods (T=3.2s), the damping effect was lower from 7% to 17%, particularly for smaller wave heights. In contrast, irregular waves showed a more pronounced reduction in wave energy, with the split chamber structure achieving up to 35% damping efficiency at a wave period of 2.4s. This suggests that irregular wave conditions allow for greater energy dissipation, likely due to their complex interaction with the chamber geometry.

Overall, the result highlights that decreasing the wave period enhances the damping capability of the split chamber structure for both regular and irregular waves. These findings suggest that Split Chamber structures can be a viable enhancement to conventional vertical breakwaters, particularly in environments where irregular wave patterns dominate. They offer a promising solution for port and coastal infrastructure where space constraints limit the use of rubble mound structures, and where high wave reflection must be minimized to improve harbor tranquility and safety.

However, the study is limited by the range of wave conditions tested and the geometric configuration of the model. The physical tests did not account for scale effects or sediment interaction, and resonance phenomena were not fully explored. Additional experiments and numerical modeling under broader wave spectra and structural parameters are needed to explore resonance effects and complex wave-structure interactions. Future work should extend the parameter space to further validate these results and optimize split chamber designs for sustainable coastal infrastructure. Future work should aim to optimize split chamber dimensions and configurations to enhance wave energy dissipation across various coastal scenarios.

Acknowledgments

This study received funding from Project Fund No. 124.01.KB.6693.SDB.001.051, which is part of the Disaster Technology Research Program of the National Research and Innovation Agency. We extend our gratitude to the management of the Hydrodynamics Technology Research Center, particularly to the researchers, engineers, laboratory technicians from the Structural Numerical Modeling Department, and all staff members who contributed to the success of this project.

References

1) M. Casas-Prat, M.A. Hemer, G. Dodet, J. Morim, X.L. Wang, N. Mori, I. Young, L. Erikson, B. Kamranzad, P. Kumar, M. Menéndez, and Y. Feng, “Wind-wave climate changes and their impacts,” Nat Rev Earth Environ, 5 (1) 23–42 (2024). doi:10.1038/s43017-023-00502-0.
2) F. Usman, Eddi Basuki Kurniawan, M. Fathoni, and M. Rozikin, “Tsunami disaster preparedness in tambakrejo village, sumbermanjing wetan distric, malang, indonesia,” Evergreen, 11 (2) 1182–1189 (2024). doi:10.5109/7183421.
3) B.G. Reguero, I.J. Losada, and F.J. Méndez, “A recent increase in global wave power as a consequence of oceanic warming,” Nat Commun, 10 (1) (2019). doi:10.1038/s41467-018-08066-0.
4) L. Nie, “Analysis of the influence of the climate change on sea level,” Applied and Computational Engineering, 3 (1) 109–115 (2023). doi:10.54254/2755-2721/3/20230363.
5) S. Yi, W. Sun, K. Heki, and A. Qian, “An increase in the rate of global mean sea level rise since 2010,” Geophys Res Lett, 42 (10) 3998–4006 (2015). doi:10.1002/2015GL063902.
6) A.S.A. Ibrahim, A.M. El-Molla, and H.G.I. Ahmed, “Long-term trends in significant wave heights in the mediterranean as an indicator of climate change,” Transactions on Maritime Science, 13 (2) (2024). doi:10.7225/toms.v13.n02.015.
7) M. Zainuddin Lubis, H. Kausarian, A. V H Simanjuntak, and Y. Handayani, “Annual Sea Surface Height Variability in the Indonesian Seas from Satellites During the 2021-2023,” 2024. https://data.marine.copernicus.eu/.
8) A. Hamid, D.C. Istiyanto, R.C. Yuniardi, S.A. Aziiz, Y.T.D. Harita, A.B. Widagdo, S.A. Latief, I. Wulandari, and R. Firmansyah, “Structural Performance of Parallel Concrete Panel Container Towards Green Coastal and Port’s Retaining Wall: A Comparison of Tie Rod Configurations,” 2024.
9) P. Taneja, G. van R. van der Kloot, and M. van Koningsveld, “Sustainability performance of port infrastructure—a case study of a quay wall,” Sustainability (Switzerland), 13 (21) (2021). doi:10.3390/su132111932.
10) N. Rangel-Buitrago, W.J. Neal, and V.N. de Jonge, “Risk assessment as tool for coastal erosion management,” Ocean Coast Manag, 186 (2020). doi:10.1016/j.ocecoaman.2020.105099.
11) Z. Huang, Y. Li, and Y. Liu, “Hydraulic performance and wave loadings of perforated/slotted coastal structures: a review,” Ocean Engineering, 38 (10) 1031–1053 (2011). doi:10.1016/j.oceaneng.2011.03.002.
12) T.I. Koutrouveli, E. Di Lauro, L. Das Neves, T. Calheiros-Cabral, P. Rosa-Santos, and F. Taveira-Pinto, “Proof of concept of a breakwater-integrated hybrid wave energy converter using a composite modelling approach,” J Mar Sci Eng, 9 (2) 1–27 (2021). doi:10.3390/jmse9020226.

13) B. Zanuttigh, and J.W. van der Meer, "Wave reflection from coastal structures in design conditions," Coastal Engineering, 55 (10) 771–779 (2008). doi:10.1016/j.coastaleng.2008.02.009.
14) R.A. Rachman, and M. Wibowo, "Kajian sedimen tersuspensi di muara sungai jelitik untuk mendukung pengembangan kawasan ekonomi khusus sungailiat, kabupaten bangka," Buletin Oseanografi Marina, 11 (3) 255–262 (2022). doi:10.14710/buloma.v11i3.41125.
15) R.A. Rachman, and M. Wibowo, "KAJIAN karakteristik sedimen dasar untuk mendukung rencana pembangunan pelabuhan patimban," JURNAL GEOLOGI KELAUTAN, 17 (2) (2019). doi:10.32693/jgk.17.2.2019.592.
16) S. Booshi, and M.J. Ketabdari, "Modeling of solitary wave interaction with emerged porous breakwater using plic-vof method," Ocean Engineering, 241 (2021). doi:10.1016/j.oceaneng.2021.110041.
17) M. Aliyari, E. Amini, R. Attarnejad, and R. Marsooli, "Contribution of coastal structures to wave force attenuation: a numerical investigation of fluid-structure interaction for partially perforated caissons," Ocean Engineering, 280 (2023). doi:10.1016/j.oceaneng.2023.114745.
18) B. Tagliafierro, A.J.C. Crespo, J. González-Cao, C. Altomare, J. Sande, E. Peña, and M. Gómez-Gesteira, "Numerical modelling of a multi-chambered low-reflective caisson," Applied Ocean Research, 103 (2020). doi:10.1016/j.apor.2020.102325.
19) A.S. Koraim, "Hydrodynamic characteristics of slotted breakwaters under regular waves," J Mar Sci Technol, 16 (3) 331–342 (2011). doi:10.1007/s00773-011-0126-1.
20) G. E. JARLAN, "A perforated vertical wall breakwater," The Dock and Harbour Authority, 0 (486) 394–398 (1961).
21) S. Takahashi, "Design of Vertical Breakwaters," Japan, 2002.
22) M.M. Han, and C.M. Wang, "Potential flow theory-based analytical and numerical modelling of porous and perforated breakwaters: a review," Ocean Engineering, 249 (2022). doi:10.1016/j.oceaneng.2022.110897.
23) C.P. Tsai, C.H. Ko, and Y.C. Chen, "Investigation on performance of a modified breakwater-integrated owc wave energy converter," Sustainability (Switzerland), 10 (3) (2018). doi:10.3390/su10030643.
24) A. Sandy Dwi Marta, W. Kongko, A. Taufiqur Rohman, A. Wibowo, and I. Yahya Ikhsanudin, "The Influence of Wave Characteristics, Tides, and Installation Conditions of L-Shaped OWC Wave Energy Converter on Energy Absorption Capability," 2024.
25) H. Khoirunnisa, W. Kongko, A. Sandy Dwi Marta, T. Budi Pratomo, A. Nurwijayanti, S. Husrin, F. Mafazi Giska Putra, D. Ariyanto, and K. Setia Wardani, "Physical Modelling Scenarios of Tsunami Wave Attenuation Induced by Variation of Mangrove Protection Width and Sea Dike," 2024.
26) M.A. Santoso, Y. Wijayanti, R.B. Prasetyo, O. Setyandito, Nizam, Aprijanto, A. Subandriya, A.T. Kurniawan, A. Sudaryanto, and B. Sutejo, "A mini review: wave energy converters technology, potential applications and current research in indonesia," Evergreen, 10 (3) 1642–1650 (2023). doi:10.5109/7151712.
27) G.S. Bennett, P. Mciver, and J. V Smallman, "A mathematical model of a slotted wavescreen breakwater," Coastal Engineering, 18 231–249 (1992).
28) K.D. Suh, and S. Park, "Wave reflection perforated-wall caisson from breakwaters," 1995.
29) K.D. Suh, J.K. Park, and W.S. Park, "Wave reflection from partially perforated-wall caisson breakwater," Ocean Engineering, 33 (2) 264–280 (2006). doi:10.1016/j.oceaneng.2004.11.015.
30) X. Liu, and Y. Liu, "Experimental study of irregular wave reflection by a perforated caisson breakwater under wave overtopping conditions," Journal of Ocean University of China, 21 (4) 926–934 (2022). doi:10.1007/s11802-022-4964-8.
31) J.I. Lee, and S. Shin, "Experimental study on the wave reflection of partially perforated wall caissons with single and double chambers," Ocean Engineering, 91 1–10 (2014). doi:10.1016/j.oceaneng.2014.08.008.
32) J Kirkegaard, G Wolters, J Sutherland, R Soulsby, L Frostick, S McLelland, T Mercer, and H Gerritsen, "IAHR Design Manual - Users Guide to Physical Modelling and Experimentation - Experience of the HYDRALAB Network," CRC Press, Boca Raton, FL, 2011. www.iahr.org.
33) G. Wolters, M. Gent, W. Allsop, L. Hamm, and D. Muhlestein, "HYDRALAB III: Guidelines for physical model testing of rubble mound breakwaters," in: Coasts, Marine Structures and Breakwaters: Adapting to Change - Proceedings of the 9th International Conference, ICE Publishing, 2009: pp. 659–670.
34) HR Wallingford Ltd, "Laboratory instrumentation and software," (n.d.).
35) E.J. Pereira, H.M. Teh, L.S. Manoharan, and C.H. Lim, "Design Optimization of a Porous Box-Type Breakwater Subjected to Regular Waves," in: MATEC Web of Conferences, EDP Sciences, 2018. doi:10.1051/matecconf/201820301018.
36) F. He, and Z. Huang, "Using an oscillating water column structure to reduce wave reflection from a

vertical wall," J Waterw Port Coast Ocean Eng, 142 (2) (2016). doi:10.1061/(asce)ww.1943-5460.0000320.

37) V.Ş. Özgür KIRCA, and M. Sedat KABDAŞLI, "Reduction of non-breaking wave loads on caisson type breakwaters using a modified perforated configuration," Ocean Engineering, 36 (17–18) 1316–1331 (2009). doi:10.1016/j.oceaneng.2009.09.003.
38) F. Husain, M.R. Alwi, and Ashury, "Efficacy of Water Chamber Type Seawall to Dissipate Incident Wave and Its Performance to Extract Wave Power," in: IOP Conf Ser Earth Environ Sci, Institute of Physics Publishing, 2018. doi:10.1088/1755-1315/135/1/012002.
39) E. Dhanunjaya, V. Venkateswarlu, and E.S. Rayudu, "Oblique wave trapping by a permeable wall breakwater connected with thick surface porous layer," Ships and Offshore Structures, 19 (5) 594–609 (2024). doi:10.1080/17445302.2023.2195241.